Tree Rings Reveal ENSO in the Last Millennium

Edward R Cook[1] and Mark A Cane[1]

[1]Affiliation not available

April 25, 2024

Tree Rings Reveal ENSO in the Last Millennium

By

Edward R. Cook
Lamont-Doherty Earth Observatory
Palisades, NY 10964

Mark A. Cane
Lamont-Doherty Earth Observatory
Palisades, NY 10964

Key Points

1. Tree-ring series from ENSO rainfall impact regions reconstruct the tropical Pacific SST field with a high degree of skill back to 1100 CE.

2. Two very different reconstruction methods produce similar results and each can only reconstruct the leading EOF mode of SST variability.

3. Reconstructions extending back 1100 CE do not reveal any clear increase in El Niño variability, but do show a recent overall SST warming.

Abstract

We present new climate field reconstructions (CFR) of tropical Pacific ENSO sea surface temperatures (HadISST) for the boreal winter season using a circum-Pacific tree-ring network from known El Niño rainfall impact regions. We used two different CFR methods: Point-by-Point Regression (PPR) and reduced-space Orthogonal Spatial Regression (OSR). Both methods have high levels of validation skill as far back as 1100 CE and exceptional skill back to 1500 CE. OSR is preferred because it has less spatial noise and is more efficient. Only the leading EOF of the SST field (EOF1) can be reconstructed with a very high level of skill; EOF2 does not validate using either method. The success of EOF1 reflects its importance for ENSO rainfall impacts; the failure with EOF2 reflects the lack of these impacts. EOF1 is shown to allow reconstruction of many ENSO indices, including the nonlinear ENSO Longitudinal Index (ELI).

Plain Language Summary

Earth's climate is strongly affected by how warm the tropical Pacific Ocean 'El Niño' region is. This is especially true for the delivery of rainfall over many parts of the globe. Tree growth can thus be strongly affected by rainfall impacts of El Niños. We use this relationship to reconstruct tropical Pacific sea surface temperatures associated with El Niño over most of the past millennium from a network of annual tree-ring chronologies located in regions known to be impacted by El Niño rainfall. Only the leading mode of variability in Pacific sea surface temperatures associated with El Niño can be reconstructed well, but it reflects most of the long-term variability of El Niño exceptionally well. The reconstruction extends back to 1500 with exceptional skill and back to 1100 with acceptable skill. We can thus compare recent El Niño variability, perhaps affected by global warming, with what happened over the previous centuries unaffected by human activity. We do not find clear evidence for an increase in El Niño activity, just an overall warming due to recent global warming.

Index terms and keywords

4922 El Nino

4920 Dendrochronology

4215 Climate and interannual variability

3305 Climate change and variability

1807 Climate impacts

1. Introduction

Since anyone choosing to read this paper is aware of the global importance of the El Niño Southern Oscillation (ENSO), we dispense with that part of the introduction (see, e.g. Sarachik and Cane (2010) and McPhaden et al. (2020) for comprehensive reviews of ENSO). The somewhat trustworthy record of ENSO – the one based on instrumental data – extends back only until the mid-19th Century (e.g. Kaplan et al., 1998). Since an El Niño event occurs roughly every 4 years on average, this record provides only ~40 cycles. These recurrences show great variability in frequency and amplitude from decade to decade; differences in spatial pattern as well. The purpose of this paper is to develop a gridded field reconstruction of tropical Pacific SSTs to extend the record of ENSO variability back to 1100 CE (or 1500 CE for a more precise product) to better characterize this variability. This new product, which builds upon past climate field reconstructions of tropical Pacific SSTs (e.g. Evans et al., 2002; Furtado et al., 2009; Emile-Geay et al., 2013), excels in a wide range of validation tests.

An inescapable question for anything climate related is how it will be affected by global warming. Though there is no firm consensus, the current leading answer is that ENSO events will become stronger and more frequent in the future (e.g. Cai et al., 2018). This projection is necessarily based on Earth System Models (ESMs), the same models that have failed to match the observed record in the tropical Pacific since 1950, when the global warming signal begins to emerge from the natural background (e.g. Seager et al 2019, 2022).

This paper is about observations and does not mention ESMs again. We extend the record of ENSO back to 1100 CE by inferring the state of the tropical Pacific from ENSO sensitive tree ring records associated with regional rainfall impacts. Then we use the ENSO SST field reconstruction to look at changes in ENSO variability over time as expressed by the ENSO Longitudinal Index (ELI) of Williams and Patricola (2018). Perhaps the past will shed light on ENSO's future.

2. Data and Methods

We aim to skillfully reconstruct tropical Pacific sea surface temperatures (SSTs) from tree ring records over the past millennium. Accordingly, two types of data are used: (1) moisture-sensitive tree-ring records used for developing circum-Pacific drought atlases (Cook et al., 2004, 2010; Palmer et al., 2015; Stahle et al., 2016; Morales et al., 2020); (2) SSTs in the tropical Pacific region of (10N-10S, 80W-160E) from the 1°x1° HadISST analysis (Rayner et al., 2003) (henceforth HAD). Globally, many thousands of tree-ring series are available as candidate predictors of the ~150 years of SSTs since 1870. As a first step to address the common problem of overfitting we reduce the predictor set by statistical screening as described in SI Methods. We are then left with 544 chronologies from 1800 diminishing to 81 from 1100.

We target only the boreal winter (DJF) season SST, when ENSO has the strongest effect on global climate. To calibrate our reconstructions, we use SST data from 1930 through 2000, after which the number of chronologies diminishes considerably. SST data from 1871 up to 1929 are withheld to validate the tree-ring estimates. We check results against other SST datasets derived from instrumental records (ERSST5, Huang et al., 2017; KAP, Kaplan et al., 1998) and find no substantive changes in validation skill (Table S1).

We regress the target SSTs on the tree ring data using two different climate field reconstruction methods. PPR (Point by Point Regression; Cook et al 1999) individually predicts the SST in each of the 2397 1°x1° grid boxes in the target domain. The other, OSR (Orthogonal Spatial Regression; Briffa et al., 1986), first rotates the SST data over the calibration period into a set of EOFs and individually predicts the principal component (PC) associated with each EOF. Individual grid point SSTs are obtained by back-transforming from EOF space. Since there can be no more than 71 EOFs from data spanning 1930-2000 and far fewer account for most of the variance, OSR will involve many fewer individual predictions than PPR. An open question is what more, if anything, may be recovered by the more computationally intensive PPR method. For OSR, we base the EOFs on the correlation matrix of the HAD grid points rather than the covariance matrix in order to give more weight to warmer points, which typically have less variance but more influence on teleconnected impacts. Results using covariance-based EOFs do not differ greatly (not shown).

In order to take full advantage of the longer tree-ring chronologies available for reconstruction, and thus produce the longest well-validated ENSO field reconstruction possible, PPR and OSR will be applied multiple times in a stepwise "nested" fashion to allow each reconstruction to be extended back in time as shorter tree-ring chronologies became unavailable. For both PPR and OSR the starting year of each reconstruction nest (tree rings over a fixed common interval) steps back at 100 year intervals, beginning in 1800 and extending back to 1100 CE, with the calibration and validation skill of each new model individually evaluated. We label these reconstructions R18, R17, … R11. Prior to 1100 the reconstruction does not validate due to the loss of ENSO-sensitive chronologies from Southeast Asia (Buckley et al., 2017).

2.1. OSR vs. PPR methods of reconstruction

OSR invites us to reconstruct only a limited number of SST EOFs. As only three of the HAD EOFs for our target region are distinct according to the 'North test' (North et al., 1982; Figure S2) we initially reconstruct the first three EOFs using OSR, cumulatively accounting for 88.4% of the total SST field variance. Taking HAD as "truth", Figure 1 (top) shows maps of the OSR and PPR calibration and validation statistics using tree-ring chronologies available from 1800 (R18). Both methods have high skill except at the western end of the domain, and, for validation, at the southeast, but OSR skill is high over a larger area. OSR shows less small-scale variability, a benefit of reduced space smoothing. Overall, Figure 1 shows that OSR performs slightly better than PPR; the far greater computational burden of PPR failed to add desirable features.

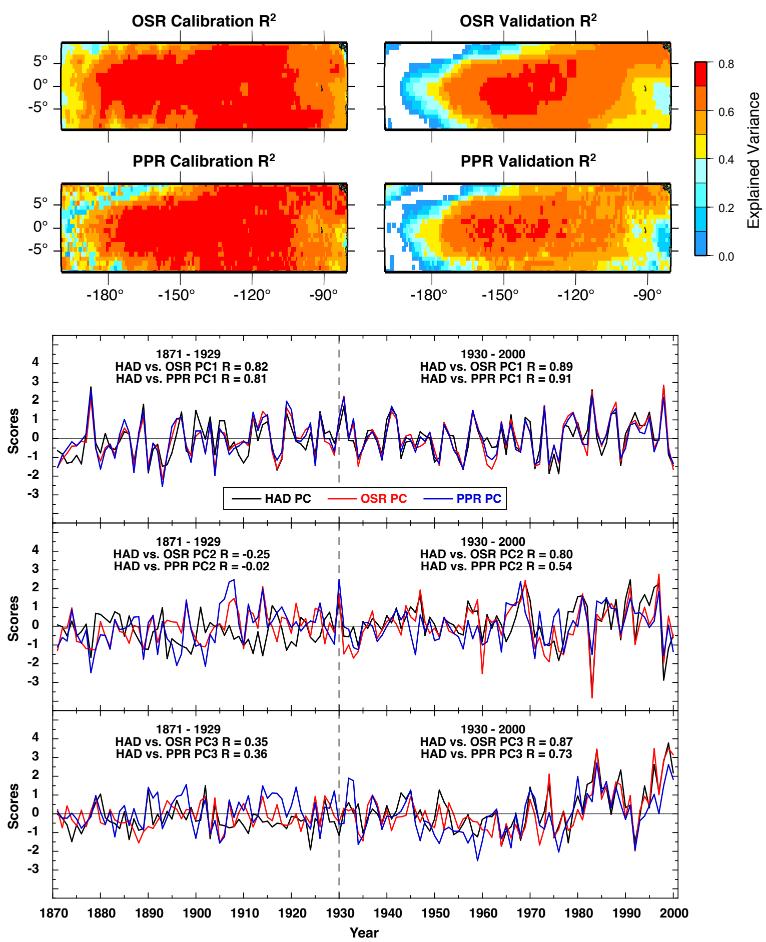

Figure 1. Top shows maps of the OSR and PPR calibration and validation statistics for the R18 tree-ring chronology nest. Their respective calibration/validation maps agree very well in pattern and magnitude over most of the target domain. The bottom plots compare the three principal components (PC1, PC2, PC3) corresponding to the EOFs from the OSR and PPR reconstructions with the PCs of HAD over the calibration (1930-2000) and the validation (1871-1929) periods. Only OSR and PPR PC1 validate well.

The PPR method takes no account of the spatial correlations within the domain; does it recover them? To determine that we examine the EOFs and associated PCs of the HAD, OSR, and PPR fields over 1871-2000. By construction, OSR EOFs are very similar to HAD EOFs (Figure S3). PPR, which is not constrained *a priori* to match the HAD EOFs is nonetheless, also similar to HAD. For HAD and OSR the first three EOFs are distinct (Figure S2). For the PPR method only the first EOF is distinct, revealing its inability to recover long-range spatial structure.

Figure 1 (bottom) compares the corresponding three PCs from the OSR and PPR reconstructions with the PCs of HAD over the calibration (1930-2000) and validation (1871-1929) periods. PC1 from either is very highly correlated with HAD PC1 for both the calibration period (R~0.90) and the validation period (R~0.80). PC2 and PC3 calibration period correlations are also high, but the validation statistics are clearly non-significant for PC2 and weak for PC3. Experiments with other ways of selecting predictors did not improve things. Both reconstruction methods are guilty of overfitting PC2 and PC3 in the calibration step. In summary, both OSR and PPR do an excellent job of reconstructing the first PC from tree rings, but only the first PC. They do only one thing, but do it very well.

It may be that our methodology is at fault for the failure to capture more than the first PC. However, the predictors we use are not *in situ* in the tropical Pacific, but rely on rainfall impacts distant from this target region. The influencers are likely to be large scale and not subtle, so it is plausible that only a single pattern, one most representative of ENSO, can be recovered by inverting ENSO's influence on tree growth. Figure 2 supports this idea. PC1 is connected to rainfall in many parts of the world where we have tree-ring chronologies (Figure S1). In contrast, PC2 has little connection to rainfall except weakly in central Africa where there are no tree ring chronologies. This lack of correlation holds for the HAD instrumental data as well. We conclude that only PC1 can be reconstructed from moisture sensitive tree-ring records. No other PC has a substantial relation to rainfall.

The top bar chart in Figure 3 shows the calibration, validation and overall skill of reconstructions of HAD NINO3.4 using PC1 from trees available (numbers in parentheses) for R18, R17, … R11. It also shows the correlation based on HAD PC1. The correlation of HAD PCI with HAD NINO3.4 is 0.98 even for the validation period; i.e., PC1 and NINO3.4 are effectively the same. There is also little change in skill among the reconstructions back to 1500. In fact, the highest R (0.83 for the validation period) is for the R15 reconstruction, though the differences among them are not significant. There is very little difference in skill between the calibration and validation periods, indicating that the calibration model is not overfitted. Before 1500 skill decreases and validation skill is visibly less then calibration skill. Nonetheless, the reconstruction back to 1100 accounts for 50% of the validation period variance, which is still useful. The R15 and R11 reconstructions are further validated against ERSST and KAP SST data (Table S1) and the results are totally consistent with what is reported in Figure 3.

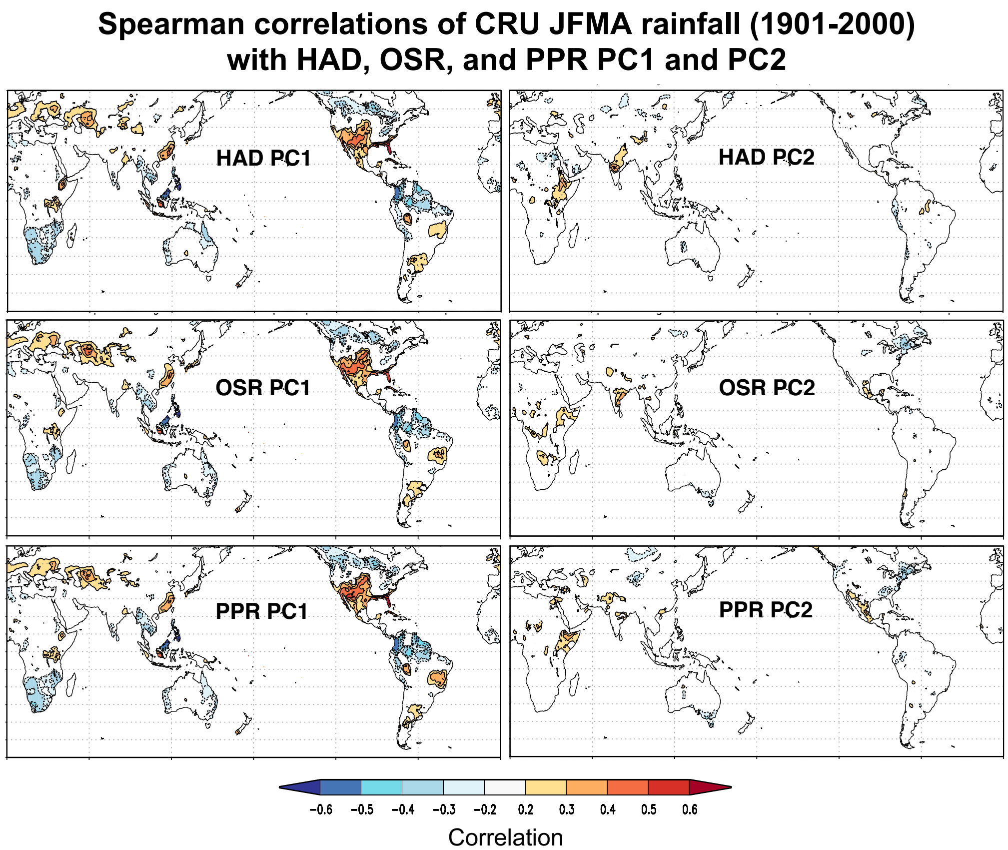

Figure 2. Rainfall correlations with HAD, OSR, and PPR PC1 and PC2. Only PC1 shows strong correlations with rainfall over areas where the trees used for reconstruction are located. In contrast, PC2 has very little correlation with rainfall globally and almost none where the trees used are growing.

The bottom bar chart in Figure 3 displays reconstructions of various common ENSO indices from HAD or R15. In addition to those on PC1 only, regressions on PC1 plus $PC1^2$ allow for nonlinear relations. For HAD we also do regressions on PC1 plus PC2 to see what is lost with the reconstructions by not having PC2. Using HAD PC1 allows a near total account of NINO3 and NINO3.4; PC1 is essentially interchangeable with these indices. It adds little to include PC2 or $PC1^2$ in the regression. NINO1+2 and NINO4 are slightly improved by including PC2, and adding $PC1^2$ to PC1 is almost as good. With R15 PC1 the correlations for NINO3, NINO3.4 and NINO4 are above 0.8 and little is gained by adding $PC1^2$, but for NINO1+2 the correlation is improved from 0.72 to 0.78 by adding $PC1^2$, compensating for the absence of PC2 in the R15 reconstruction. We also include a correlation between an estimate of the ELI from our HAD DJF target field with DJF ELI available from Williams and Patricola (2018), the latter based on ERSST data (Huang et al., 2017). The correlation (R=0.93) is extremely high.

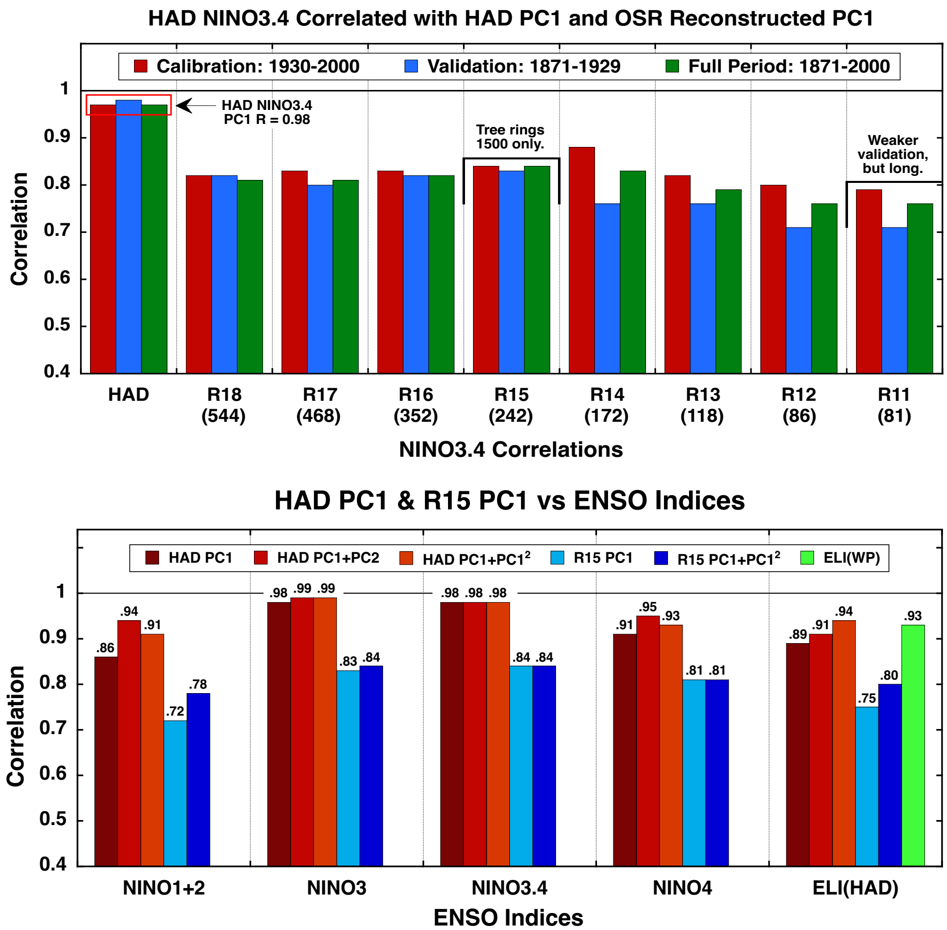

Figure 3. Top bar chart shows the calibration, validation and overall skill of reconstructions of HAD NINO3.4 using PC1 from HAD and the reconstructions based on trees available (in parentheses) in the common period nests. The R15 reconstruction is the best overall. The bottom bar chart illustrates our ability to reconstruct various commonly used ENSO indices from either regressions on the PCs from HAD or R15. Also included is a correlation between our estimate of the ELI from HAD and that available from Williams and Patricola (2018).

Global correlations of rainfall with PC1 testifies to the skill of the reconstructions. The correlation patterns for R15 and R11 (Figure S4) are very similar to that for HAD and also very similar to the PC1 rainfall correlation maps shown in Figure 2. However, this is not an entirely independent test, as much of the rainfall field overlaps geographically with the trees used in the reconstructions. In contrast, rainfall correlations over Africa, Europe, and the Middle East from HAD, R15, and R11 PC1s (Figure 4) provide a true out-of-sample comparison because no tree-ring chronologies in the area shown were used in the reconstructions. The pattern in the R15 panel is almost indistinguishable from that in the HAD panel. R11, a reconstruction with less skill, is nonetheless very close to the other two in capturing this ENSO impact on rainfall. These findings are consistent with comparisons of NINO3.4 indices estimated from CRU and GPCC teleconnected precipitation data (van Oldenborgh et al., 2021) with HAD, R15, and R11 PC1 (Figure S5). R15 has correlations >0.8 with GPCC and CRU NINO3.4 indices, which are almost the same as those for HAD. R11 correlations are lower, but still highly significant.

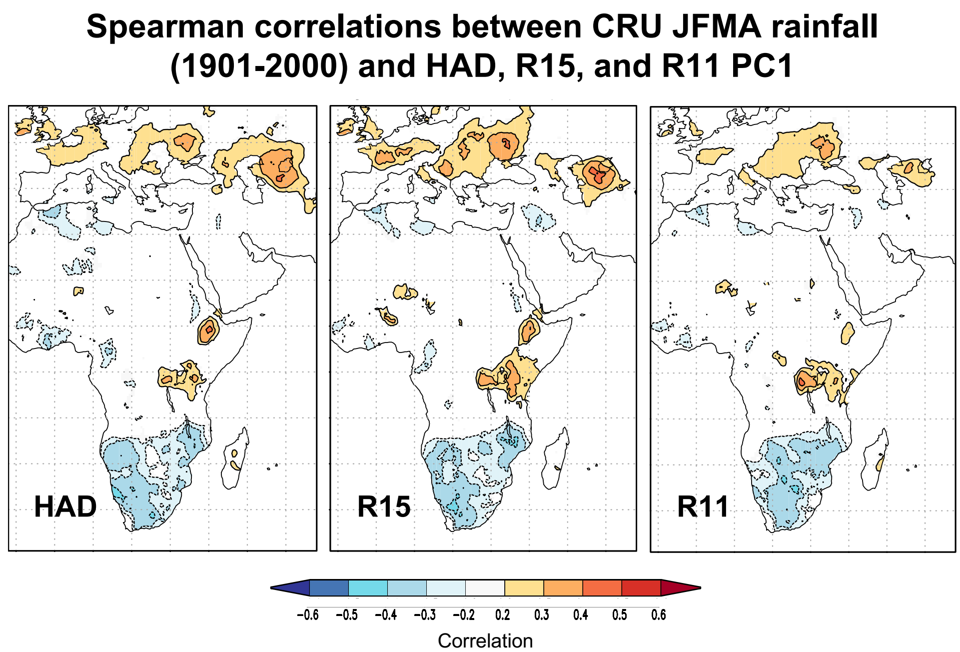

Figure 4. Rainfall correlations over Africa, Europe, and the Middle East from HAD, R15, and R11 PC1s. This is a true out-of-sample comparison because no tree-ring chronologies in the area shown were used in the reconstructions. The pattern in the R15 panel is almost indistinguishable from that in the HAD panel. R11, a reconstruction with less skill, is nearly as good.

The final ENSO index investigated here is the ELI (ENSO Longitudinal Index) of Williams and Patricola (2018; W&P). It is a continuous measure intended to capture ENSO diversity. W&P ELI has a strong quadratic relationship with HAD, R15, and R11 PC1s (Figure 3 bottom; Figure S6). (This could be anticipated in view of the relation between ELI and NINO3 shown in W&P; their Figure S6.). Given these strong relationships, we regressed our R15 and R11 PCs on W&P ELI to produce our own reconstructions of ELI back to 1500 and 1100 (Figure 5; Figure S6).

4. Summary and Discussion

We began this work with a number of questions. The overarching one was how skillfully can we reconstruct DJF tropical Pacific (ENSO) SST fields from *remote impacts* on moisture sensitive trees without any *in situ* data – any data from the tropical Pacific? While this has been done several times before for ENSO indices (e.g. Stahle et al., 1998; D'Arrigo et al., 2005; Wilson et al., 2010; Li et al., 2013), we have taken an intensive new look at it as a spatial reconstruction problem, with emphasis placed on validation testing of our estimates. The resulting reconstructions are unusually skillful. We used two different reconstruction methods: PPR uses the tree-ring chronologies to estimate each of the 2397 1°x1° SST boxes in our target area while OSR targets the leading EOFs of the SST field. Would PPR provide more information about the target SST field? It turned out that they have roughly equivalent ability (Figure 1). We settled on OSR because it is somewhat less noisy and is far less computationally demanding.

The obvious next question is how many SST EOF/PCs can we reconstruct? The answer is: just one, the leading mode. The inability to estimate PC2 from moisture sensitive trees is shown to be a consequence of the lack of any connection between rainfall and PC2 of tropical Pacific SST (Figure 2). Disappointing perhaps, but the reconstruction of this first PC is exceptionally skillful. Moreover, the leading mode accounts for almost 72% of the original SST field variance. Fortunately, PC1 is sufficient to allow excellent estimates of some common ENSO indices (NINO3, NINO3.4) and good estimates of others (NINO4, NINO1+2); see Figure 3 (bottom) and Table S1. The nonlinear ELI is also well captured by a quadratic function of PC1 (Figure S6).

How far back in time can we go with useful skill? We found little difference in skill between using all 544 chronologies from 1800 CE and using fewer than half as many (242) available back to 1500 CE (Figure 3 top). Over the validation period (1871-1929) the correlation of the instrumental HAD PC1 with this R15 reconstruction is R=0.83, accounting for almost 70% of the variance, making it one of the most skillful proxy reconstructions we know of. This out-of-calibration skill is only slightly lower than the R=0.84 for the calibration period (1930-2000), indicating that there is little overfitting. With only the 81 chronologies going back to 1100 CE the validation period correlation of R11 PC1 with HAD PC1 is 0.71, which is still high enough to be useful. The higher R (0.79) in the calibration period is indicative of some overfitting.

A virtue of our reconstructions is the precision of the tree-ring dating. All banded annual proxies – tree-rings, ice cores, corals, speleothems, lake sediments – are subject to dating errors. Annual bands can be missing or missed, intra-annual features can be counted as annual bands.

Dendrochronologists address this by replication within each chronology, which enables rigorous crossdating (Fritts, 1976). Moreover, very many chronologies go into our estimates of ENSO PC1 making it virtually certain that the annual dating of our reconstructions is correct. Replication is much more difficult with other proxies, but has been done for some, like corals (Hendy et al., 2003; Lough, 2004; DeLong et al., 2007).

Our reconstructions rely on remote impacts of tropical Pacific SST. No *in situ* information is used. We speculate that our indices are consequently robust indicators of ENSO impacts, possibly as good or better than NINO3.4 or some other SST measure for this purpose. Their relation to rainfall shown in Figure 2 and Figure 4 support this speculation, but how broadly it holds is unknown.

Figure 5 shows the R11 and R15 reconstructions of PC1 (equivalently, NINO3.4) and the ENSO Longitudinal Index (ELI) based on regression (Figure S6) back in time with smooth polynomial curves applied to highlight recent warming. While the positive excursions (i.e. El Niño events) in recent decades are higher than any seen back to 1100, the variability does not appear to be unique in the record. Rather, recent variability is riding on an unprecedented warming trend. Thus, the reconstructions suggest that ENSO variability under global warming is high, but not clearly higher than at a number of times in the past millennium. But the world is warmer, and these two impact-based indices suggest that the impacts are becoming more severe.

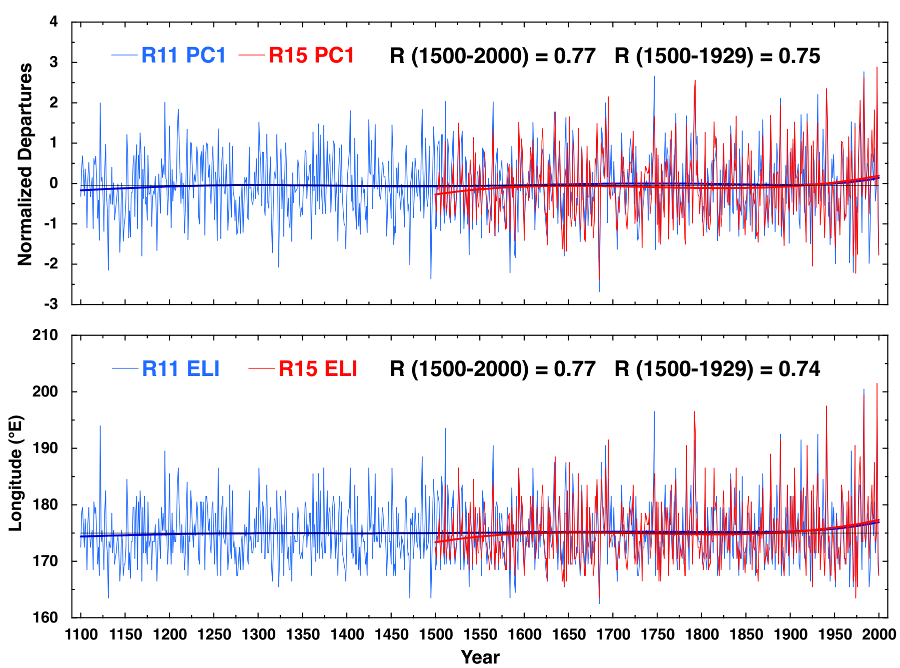

Figure 5. PC1 and ELI series based on the R15 and R11 ENSO reconstructions. Overall warming in recent decades is indicated by smooth polynomial curves. Full overlap and pre-calibration correlations are shown.

Acknowledgments

E. R. Cook and M. A. Cane acknowledge support of this research by the NSF Paleo Perspectives on Climate Change (P2C2) Program, grant AGS 20-02452 (lead P.I. A. Kaplan). ERC was responsible for producing the reconstructions and both ERC and MAC for the analyses and interpretations presented. We declare no conflicts of interest.

Open Research

The Hadley Centre Sea Ice and Sea Surface Temperature data set (HadISST) is available from https://www.metoffice.gov.uk/hadobs/hadisst/. The HadISST target field data, along with the R15 and R11 reconstructed HadISST fields, will be made available at NOAA-NCEI Paleoclimatology.

References

Briffa, K. R., Jones, P. D., Wigley, T. M. L.,Pilcher, J. R. & Baillie, M. G. L. (1986). Climate reconstruction from tree rings: Part 2, Spatial reconstruction of summer mean sea-level pressure patterns over Great Britain. *Journal of Climatology,* 6, 1–15. https://doi.org/10.1002/joc.3370060102.

Buckley, B., Stahle, D., Luu, H. T., Wang, S-Y., Nguyen, T., Thomas, P., Nam, L., Ton, T., Bui, T. & Thiet, N. (2017). Central Vietnam climate over the past five centuries from cypress tree rings. *Climate Dynamics*, 48, 3707-3723. https://doi.org/10.1007/s00382-016-3297-y.

Cai, W., Wang, G. Dewitte, B., Wu, L., Santoso, A., Takahashi, K., Yang, Y., Carréric, A. & McPhaden, M. J. (2018). Increased variability of eastern Pacific El Niño under greenhouse warming. *Nature*, 564, 201–206. https://doi.org/10.1038/s41586-018-0776-9.

Capotondi, A., Wittenberg, A., Newman, M., Di Lorenzo, E., Yu, J-Y., Braconnot, P., Cole, J., Dewitte, B., Giese, B., Guilyardi, E., Jin, F-F., Karnauskas, K., Kirtman, B., Lee, T., Schneider, N., Xue, Y. & Yeh, S-W. (2015). Understanding ENSO diversity. *Bulletin of the American Meteorological Society*, 96, 921-938. https://doi.org/10.1175/BAMS-D-13-00117.1.

Cook, E. R., Meko, D. M., Stahle, D. W., & Cleaveland, M. K. (1999). Drought reconstructions for the continental United States. *Journal of Climate*, 12, 1145-1162. https://doi.org/10.1175/1520-0442(1999)012<1145:DRFTCU>2.0.CO;2

Cook, E. R., Woodhouse, C., Eakin, C. M., Meko, D. M. & Stahle, D. W. (2004). Long-term aridity changes in the western United States. *Science*, 306, 1015-1018. https://doi.org/10.1126/science.1102586.

Cook, E. R., Anchukaitis, K. J. Buckley, B. M., D'Arrigo, R. D., Jacoby, G. C. & Wright, W. E. (2010). Asian monsoon failure and megadrought during the last millennium. *Science*, 328(5977), 486-489. https://www.science.org/doi/10.1126/science.1185188.

D'Arrigo, R., Cook, E., Wilson, R., Allan, R., & Mann, M. (2005). On the variability of ENSO over the past six centuries. *Geophysical Research Letters*, 32(3), L03711. https://agupubs.onlinelibrary.wiley.com/doi/10.1029/2004GL022055.

DeLong, K., Quinn, T. & Taylor, F. (2007). Reconstructing twentieth-century sea surface temperature variability in the southwest Pacific: A replication study using multiple coral Sr/Ca records from New Caledonia. *Paleoceanography and Paleoclimatology*, 22(4), PA4212. https://doi.org/10.1029/2007PA001444.

Emile-Geay, J., Cobb, K., Mann, M. & Wittenberg, A. (2013). Estimating central equatorial Pacific SST variability over the past millennium. Part II: reconstructions and implications. *Journal of Climate*, 26(7), 2329-2352. https://doi.org/10.1175/JCLI-D-11-00511.1.

Evans, M., Kaplan, A. & Cane, M. (2002). Pacific sea surface temperature field reconstruction from coral **$\delta^{18}O$** data using reduced space objective analysis. *Paleoceanography and Paleoclimatology*, 17(1), 7-1-713, https://agupubs.onlinelibrary.wiley.com/doi/10.1029/2000PA000590.

Fritts, H. C. (1976). *Tree Rings and Climate*. Academic Press, New York. 567 pp.

Furtado, J., Di Lorenzo, E., Cobb, K. & Bracco, A. (2009). Paleoclimate reconstructions of tropical sea surface temperatures from precipitation proxies: methods, uncertainties, and nonstationarity. *Journal of Climate*, 22, 1104-1123. https://journals.ametsoc.org/view/journals/clim/22/5/2008jcli2415.1.xml.

Hendy, E., Gagan, M., & Lough, J. (2003). Chronological control of coral records using luminescent lines and evidence for non-stationary ENSO teleconnections in northeast Australia. *The Holocene*, 13(2), 187-199. https://journals.sagepub.com/doi/10.1191/0959683603hl606rp.

Huang, B., Thorne, P., Banzon, V., Boyer, T., Chepurin, G., Lawrimore, J., Menne, M., Smith, T., Vose, R. & Zhang, H-M. (2017). Extended reconstructed sea surface temperature, version 5 (ERSSTv5): upgrades, validations, and intercomparisons. *Journal of Climate*, 30(20), 8179–8205. https://journals.ametsoc.org/view/journals/clim/30/20/jcli-d-16-0836.1.xml.

Kaplan, A., Cane, M. A., Kushnir, Y., Clement, A. C., Blumenthal, M. B. & Rajagopalan, B. (1998). Analyses of global sea surface temperature 1856–1991. *Journal of Geophysical Research,* 103(C9), 18567-18589. https://agupubs.onlinelibrary.wiley.com/doi/10.1029/97JC01736.

Lenssen, N., Goddard, L. & Mason, S. (2020). Seasonal forecast skill of ENSO teleconnection maps. *Weather and Forecasting*, 35(6), 2387–2406. https://doi.org/10.1175/WAF-D-19-0235.1.

Lough, Janice. (2004). A strategy to improve the contribution of coral data to high-resolution paleoclimatology. *Palaeogeography, Palaeoclimatology, Palaeoecology*, 204(1-2), 115-143. https://www.sciencedirect.com/science/article/abs/pii/S0031018203007272?via%3Dihub.

McPhaden, M., Santoso, A. & Cai, W. (Eds.). (2020). *El Niño Southern Oscillation in a Changing Climate*. DOI:10.1002/9781119548164.

Morales, M. S., Cook, E. R., Barichivich, J., Christie, D. A., Villalba, R., LeQuesne, C., Srur, A., Ferrero, E., Masiokas, M., Gonzalez-Reyes, A., Couvreux, F., Matskovsky, V., Aravena, J. C., Lara, A., Urrutia, R., Mundo, I. A., Muñoz, A., Bianchi, L., Rodriguez-Catón, M., Lopez, L., Rojas, F., Prieto, M. R., Rojas-Badilla, M., Alvarez, C., Smerdon, J. E., Luckman, B., Lister, D., Harris, I., Jones, P. D., Velazquez, G., Alistee, D., Aguilera, I., Marcotti, E., Williams, A. P., & Boninsegna, J. (2020). Six hundred years of South American tree rings reveal an increase in severe hydroclimatic events since mid-20th century. *Proceedings of the National Academy of Sciences USA,* 117(29), 16816-16823. https://www.pnas.org/doi/full/10.1073/pnas.2002411117.

North, G., Bell, T. Cahalan, R. & Moeng, F. (1982). Sampling errors in the estimation of empirical orthogonal functions. *Monthly Weather Review*, 110(7), 699-706. https://doi.org/10.1175/1520-0493(1982)110%3C0699:SEITEO%3E2.0.CO;2.

Palmer, J. G., Cook, E., Turney, C., Allen, K., Fenwick, P., Cook, B., O'Donnell, A., Lough, J., Grierson, P. & Baker, P. (2015). Drought variability in the eastern Australia and New

Zealand summer drought atlas (ANZDA, CE 1500-2012) modulated by the Interdecadal Pacific Oscillation. *Environmental Research Letters*, 10(12), 124002. https://iopscience.iop.org/article/10.1088/1748-9326/10/12/124002.

Rayner, N. A., Parker, D. E., Horton, E. B., Folland, C. K., Alexander, L. V., Rowell, D. P. (2003). Global analyses of sea surface temperature, sea ice, and night marine air temperature since the late nineteenth century. *Journal of Geophysical Research*, 108(D14). https://doi.org/10.1029/2002JD002670.

Sarachik, E. & Cane, M. (2010). *The El Niño-Southern Oscillation Phenomenon*. Cambridge University Press. https://www.cambridge.org/core/books/el-ninosouthern-oscillation-phenomenon/DBB063CB79D4E97350B09F16B8A156A1.

Seager, R. Cane, M., Henderson, N., Lee, D-E., Abernathey, R. & Zhang, H. (2019). Strengthening tropical Pacific zonal sea surface temperature gradient consistent with rising greenhouse gases. *Nature Climate Change*, 9, 517-522. https://doi.org/10.1038/s41558-019-0505-x.

Seager, R., Henderson, N. & Cane, M. (2022). Persistent discrepancies between observed and modeled trends in the tropical Pacific Ocean. *Journal of Climate*, 35(14), 4571-4584. https://journals.ametsoc.org/view/journals/clim/35/14/JCLI-D-21-0648.1.xml.

Stahle, D. W., D'Arrigo, R. D., Krusic, P. J., Cleaveland, M. K., Cook, E. R., Allan, R. J. , Cole, J. E., Dunbar, R. B., Therrell, M. D., Gay, D. A., Moore, M. D., Stokes, M. A., Burns, B. T., Villanueva-Diaz, J., & Thompson, L. G. (1998). Experimental dendroclimatic reconstruction of the Southern Oscillation. *Bulletin of the American Meteorological Society*, 79(10), 2137–2152. https://journals.ametsoc.org/view/journals/bams/79/10/1520-0477_1998_079_2137_edrots_2_0_co_2.xml.

Stahle, D. W., Cook, E. R., Burnette, D. J., Villanueva, J., Cerano, J., Burns, J. N., Griffin, R. D., Cook, B. I., Acuna, R., Torbenson, M. C. A. & Sjezner, P. (2016). The Mexican drought atlas: tree-ring reconstructions of the soil moisture balance during the last pre-Hispanic, colonial, and modern eras. *Quaternary Science Reviews*, 149, 34-60. https://www.sciencedirect.com/science/article/abs/pii/S0277379116302244?via%3Dihub.

van Oldenborgh, G. J., Hendon, H., Stockdale, T., L'Heureux, M., Coughlan de Perez, E., Singh, R. & Aalst, M. (2021). Defining El Niño indices in a warming climate. *Environmental*

Research Letters, 16(4), 044003. https://iopscience.iop.org/article/10.1088/1748-9326/abe9ed.

Williams, I. & Patricola, C. (2018). Diversity of ENSO events unified by convective threshold sea surface temperature: a nonlinear ENSO index. *Geophysical Research Letters*, 45(17), 9236-9244. https://doi.org/10.1029/2018GL079203.

Wilson, R., Cook, E., D'Arrigo, R., Riedwyl, N., Evans, M., Tudhope, A. W., & Allan, R. (2010). Reconstructing ENSO: The influence of method, proxy data, climate forcing and teleconnections. *Journal of Quaternary Science*, 25, 62-78. https://doi.org/10.1002/jqs.1297.

Supplemental Information for

Tree Rings Reveal ENSO in the Last Millennium

Edward R. Cook[1] and Mark A. Cane[1]

[1]Lamont-Doherty Earth Observatory, Palisades, NY

Contents of this file: Methods, Table S1, Figures S1 to S6, References

Methods with Table S1, Figures S1 to S6, and References

Globally, many thousands of tree-ring series are available as candidate predictors of the ~150 years of SSTs since 1870. As a preliminary filter, we only use tree-ring records from places where ENSO has a predictable influence on rainfall (Lenssen et al., 2020; Figure S1A). There are 1239 such tree-ring chronologies in those regions at our disposal beginning on or before 1800 CE, with the number diminishing to 151 before 1100 CE. We further reduce this pool of candidate predictors by eliminating those that correlate at less than the 2-tailed 90% confidence level, this after first applying autoregressive modeling and prewhitening to both the tree rings and SSTs to avoid loss of degrees of freedom for testing due to autocorrelation (Dawdy and Matalas, 1964) and to correct for differences in short-lag persistence between tree rings and SSTs (sensu Meko, 1981; Cook et al., 1999). Screening the tree rings leaves 544 chronologies from 1800 and 81 from 1100.

Figure S1B shows as an example those chronologies beginning on or before 1500 CE that survived this screening step. Note that our ENSO reconstruction experiment based on mostly extratropical moisture sensitive tree rings departs greatly from the network of precipitation proxies used by Furtado et al. (2009) to reconstruct ENSO; their network was largely restricted to the tropics and only included five tree-ring predictors.

The OSR method requires as input the number of predictand (HAD SST) EOFs to reconstruct. We use the ‘North test’ to determine how many HAD EOFs for our target region are distinct enough to reconstruction according to the ‘North test’ (North et al., 1982; Figure S2) and estimate that this number is the three leading EOFs accounting for 88.4% of the field variance. Using this information in OSR, we reconstruct these modes of SST variability using all tree-ring chronologies that begin on or before 1800 CE and pass the screening as described above. In contrast, the PPR method does not require any spatial information from the SST field to reconstruct it because each SST grid point is reconstructed separately. But because PPR does not take account of the spatial correlations within the domain, but how well does it recover them?

To determine that we compare here the three leading EOFs of the HAD, OSR, and PPR fields and use as the basis period 1871-2000 for all data sets. For HAD the first three EOFs account for 71.8%, 12.3%, and 4.5% of the variance; after that, the EOFs are not distinct (Figure S2). For OSR the corresponding EOF percentages are 77.3, 14.6, and 6.1 and for PPR they are 77.6% and 4.8%, and 3.0%, respectively. Only PPR EOF1 is distinct in this case, thus revealing a limit to the ability of this pointwise reconstruction method to cleanly recover long-range spatial structure. But for completeness all three PPR EOFs are considered in this initial comparison.

Figure S3 shows that the OSR EOFs are very similar to the HAD EOFs. This is expected by construction since OSR explicitly targets the HAD EOFs over the 1930-2000 calibration period. In contrast, PPR is not constrained a priori to match the EOFs of the target field. Nonetheless, the PPR EOFs are also similar to those of HAD (e.g. the correlations at the bottom of Figure S3).

Figure S4 shows near-global maps of correlation between CRU JFMA rainfall and PC1 from HAD instrumental SST and the OSR and PPR R15 and R11 reconstructions. In this case only the leading EOF was reconstructed by OSR because EOF2 and EOF3 could not be reconstructed with any skill (Figure 1 in main paper). The similarities in map patterns between HAD, R15, and R11 are extremely good, which serves as another form of validation of the tree-ring reconstructions, even in the case of the weaker R11 reconstruction (Figure 3 in main paper).

Figure S5 shows correlations between NINO3.4 indices constructed from GPCC and CRU teleconnected El Niño rainfall signals (van Oldenborgh et al., 2021) and HAD, R15, and R11 PC1. Recall from the main paper (Figure 3 top) that HAD PC1 is effectively the same as the NINO3.4 index based on instrumental SST data. Here we have an alternative estimate of NINO3.4 based on teleconnected rainfall signals similar to what has enabled us to reconstruct the HAD SST field form tree rings. The HAD and R15 correlations are almost the same and the R11 correlations are weaker, but still useful. These results further validate the use of PC1 from OSR reconstruction as a robust estimate of ENSO variability extending back almost a full millennium.

Figure S6 shows the nonlinear (quadratic) relationship between HAD, R15, and R11 PC1 and the Williams and Patricola (2018; W&P) ELI for the DJF season (left-hand plot). The W&P ELI is based on ERSST data, thus making it data independent of the HadISST-based PC1s, but the fitted models are still excellent. The fitted relationships shown in Figure S6 have been used to estimate ELI from both R15 PC1 and R11 PC1 (Figure 5 in main paper).

Table S1. Calibration and validation tests of the NINO1+2, NINO3, NINO3.4, and NINO4 indices extracted from the OSR R15 and R11 EOF1 SST field reconstructions. These ENSO indices are compared to those based on HAD, ERSST, and KAP instrumental SST data. Sources of these instrumental ENSO indices used for testing are provided at the bottom. The 1930-2000 and 1871-1929 tests conform to the calibration and validation periods used for developing and testing R15 and R11. Pearson correlations are reported. R15 outperforms R11 in all cases, consistent with their OSR validation statistics in Figure 3. The weaker NINO1+2 correlations are consistent with those produced from LMR and PHYDA data assimilation SST fields (Luo et al., 2022, their Figure S4).

HAD SST ENSO DJF Indices[1]								
	NINO4		NINO3.4		NINO3		NINO1+2	
ENSO Recon	1871 1929	1930 2000	1871 1929	1930 2000	1871 1929	1930 2000	1871 1929	1930 2000
R15	0.81	0.83	0.83	0.89	0.81	0.88	0.69	0.73
R11	0.69	0.76	0.69	0.83	0.66	0.82	0.57	0.69
ERSST SST ENSO DJF Indices[1]								
	NINO4		NINO3.4		NINO3		NINO1+2	
ENSO Recon	1871 1929	1930 2000	1871 1929	1930 2000	1871 1929	1930 2000	1871 1929	1930 2000
R15	0.72	0.79	0.84	0.88	0.82	0.87	0.56	0.60
R11	0.53	0.67	0.67	0.78	0.66	0.79	0.45	0.55
KAP SST ENSO DJF Indices[2]								
	NINO4		NINO3.4		NINO3		NINO1+2	
ENSO Recon	1871 1929	1930 2000	1871 1929	1930 2000	1871 1929	1930 2000	1871 1929	1930 2000
R15	0.83	0.82	0.86	0.90	0.85	0.88	0.66	0.71
R11	0.69	0.74	0.70	0.82	0.69	0.82	0.58	0.67

HAD and ERSST NINO Indices[1]: http://climexp.knmi.nl/
KAP NINO Indices[2]: http://iridl.ldeo.columbia.edu/SOURCES/.Indices/.nino/.EXTENDED/

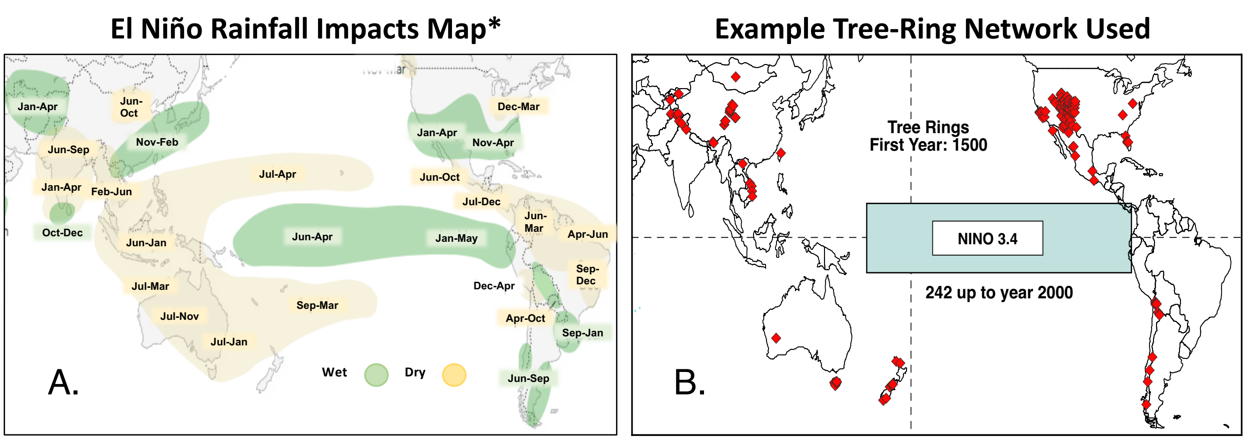

Figure S1. Rainfall impacts map (A) adapted from Lenssen et al. (2020; map downloaded from http://iridl.ldeo.columbia.edu/maproom/IFRC/FIC/ElNinoandRainfall220) and an example tree-ring network beginning in 1500 CE used to reconstruct the indicated ENSO SST target field.

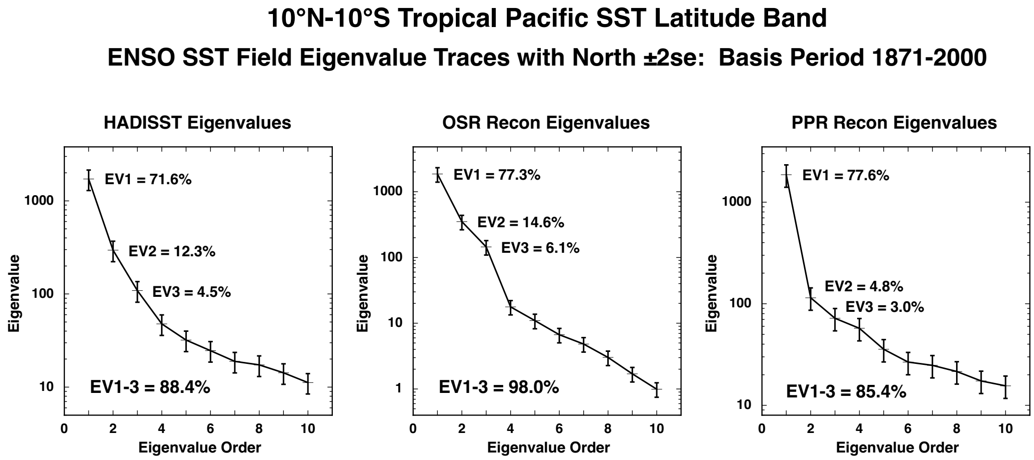

Figure S2. Eigenvalue traces of the HAD, OSR, and PPR SST fields with North ±2se limits applied to test for how many distinct EOFs can be determined. The HAD instrumental SSTs have three distinct EOFs. The OSR reconstructed SSTs have by construction three distinct EOFS because that many EOFs were chosen for reconstruction by OSR. The PPR reconstructed SSTs have only one distinct EOF, which reveals its inability to cleanly recover long-range spatial structure.

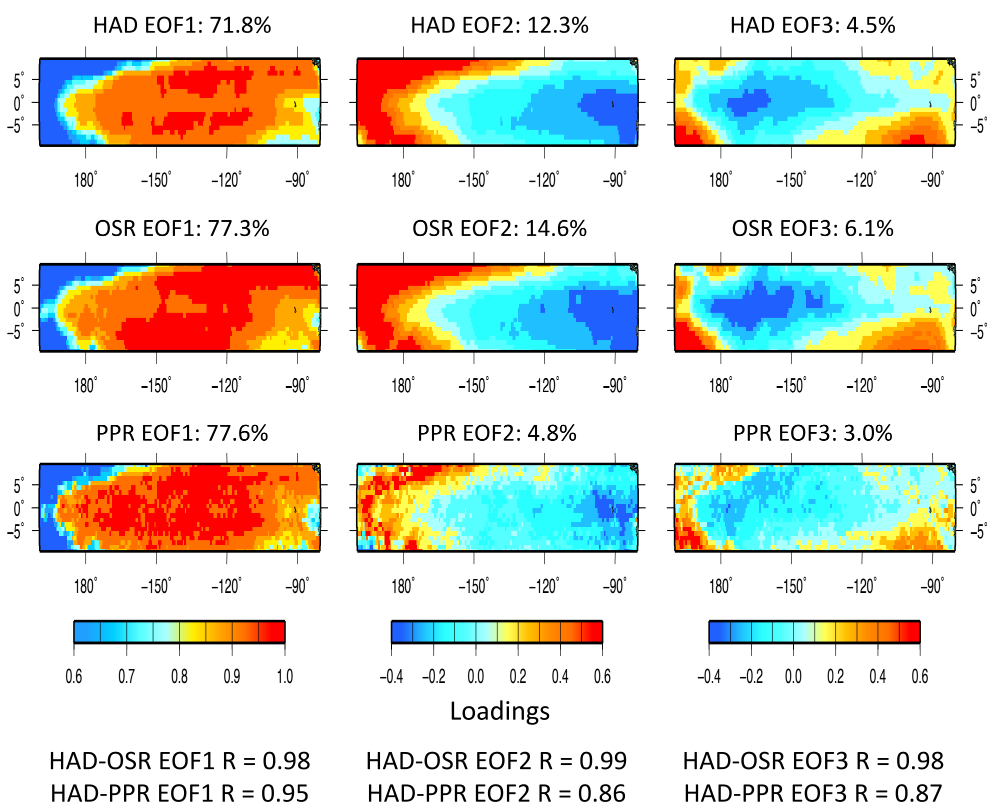

Figure S3. Comparisons of HAD, OSR, and PPR EOFs. The three OSR EOFs are almost identical to HAD by construction. However, even though only one PPR EOF is distinct (Figure S2), all three PPR EOFs are similar in pattern to the HAD EOFs (see the correlations).

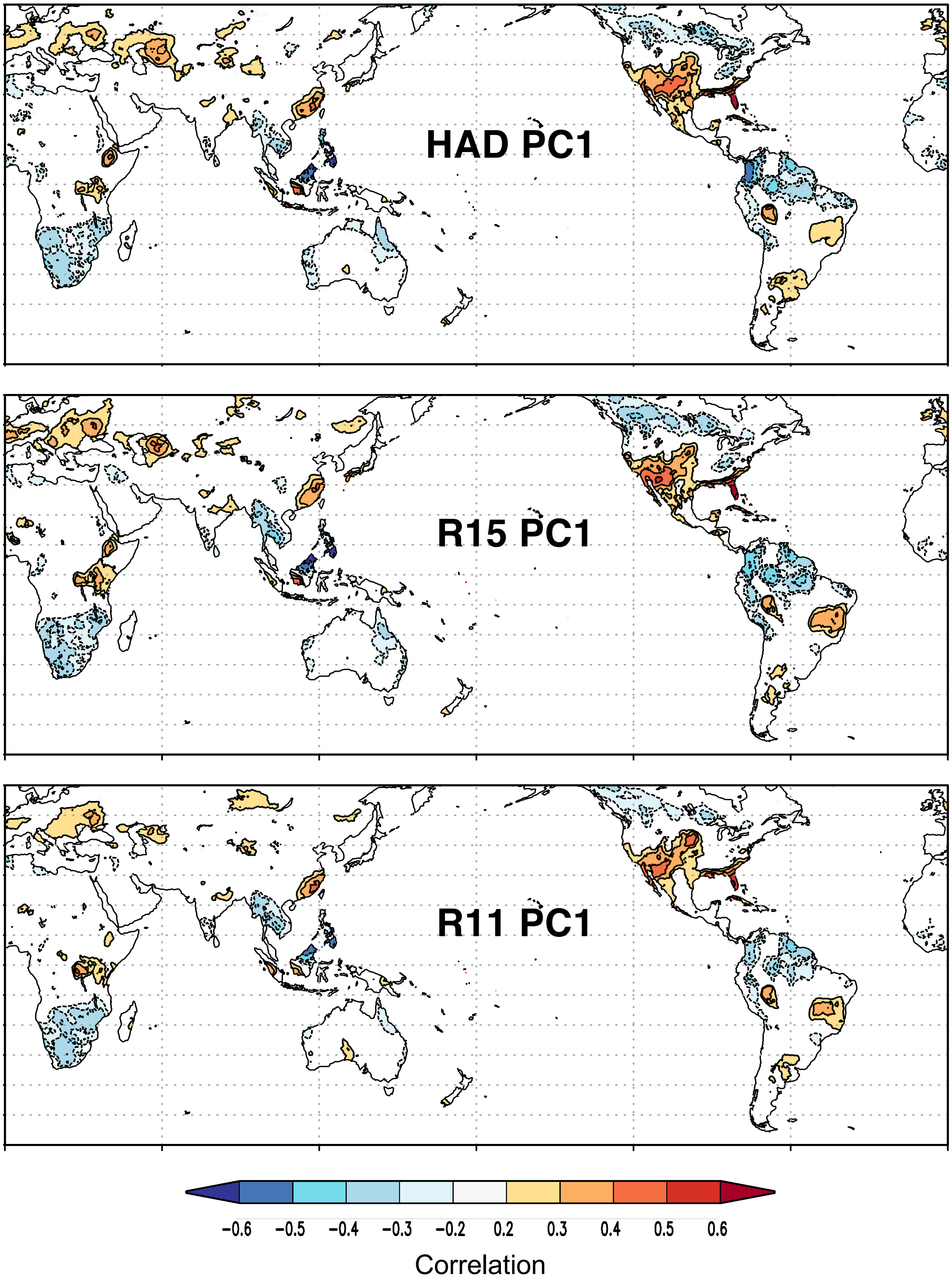

Figure S4. Maps showing the correlations between HAD, R15, and R11 PC1 with CRU JFMA precipitation (1901-2000). The patterns of correlation produced by R15 and R11 are extremely similar to that produced by PC1 of the HAD SST data.

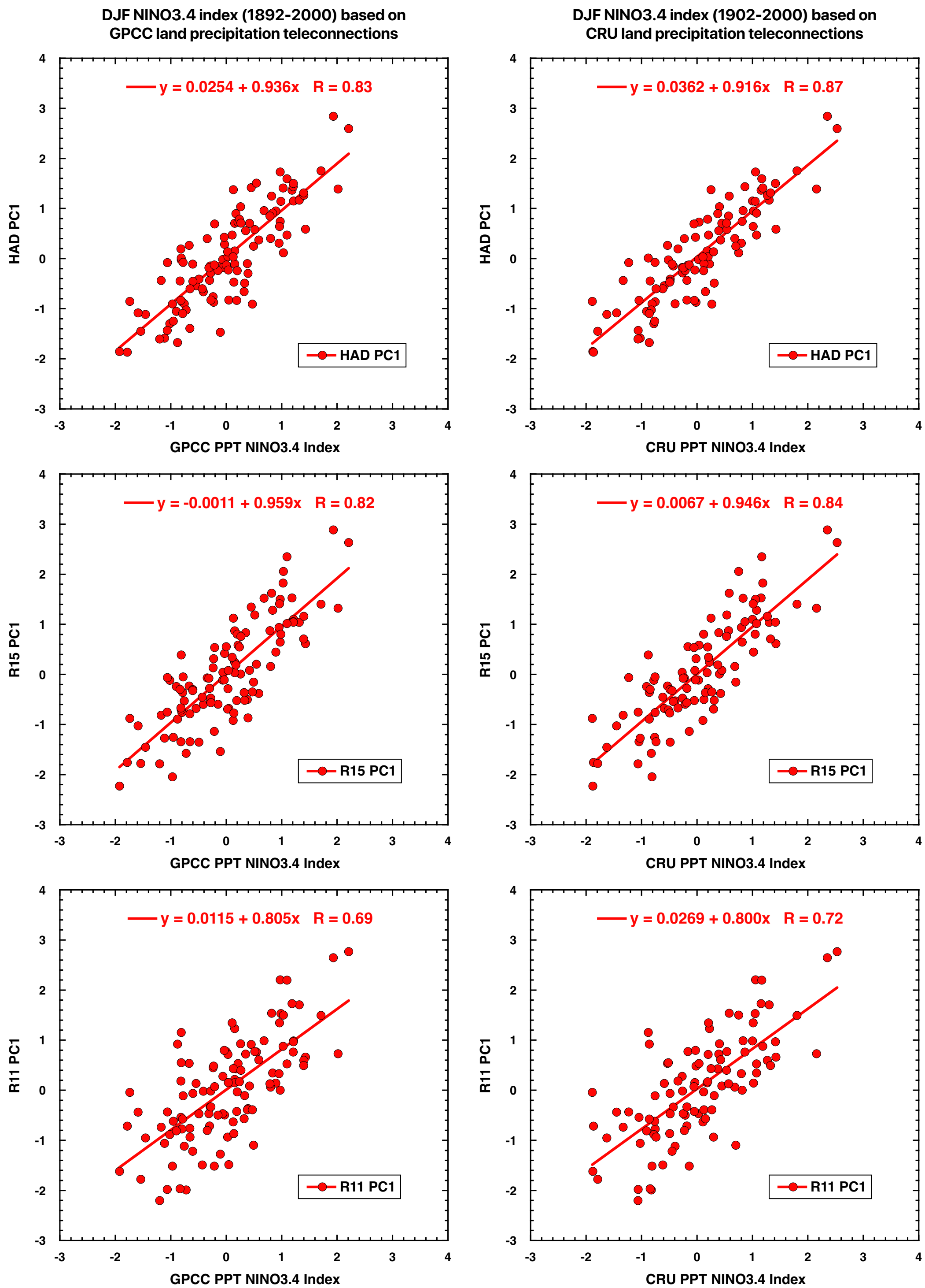

Figure S5. Correlations between NINO3.4 indices estimated from CRU and GPCC teleconnected precipitation signals (van Oldenborgh et al., 2021; https://climexp.knmi.nl/) with HAD, R15, and R11 PC1.

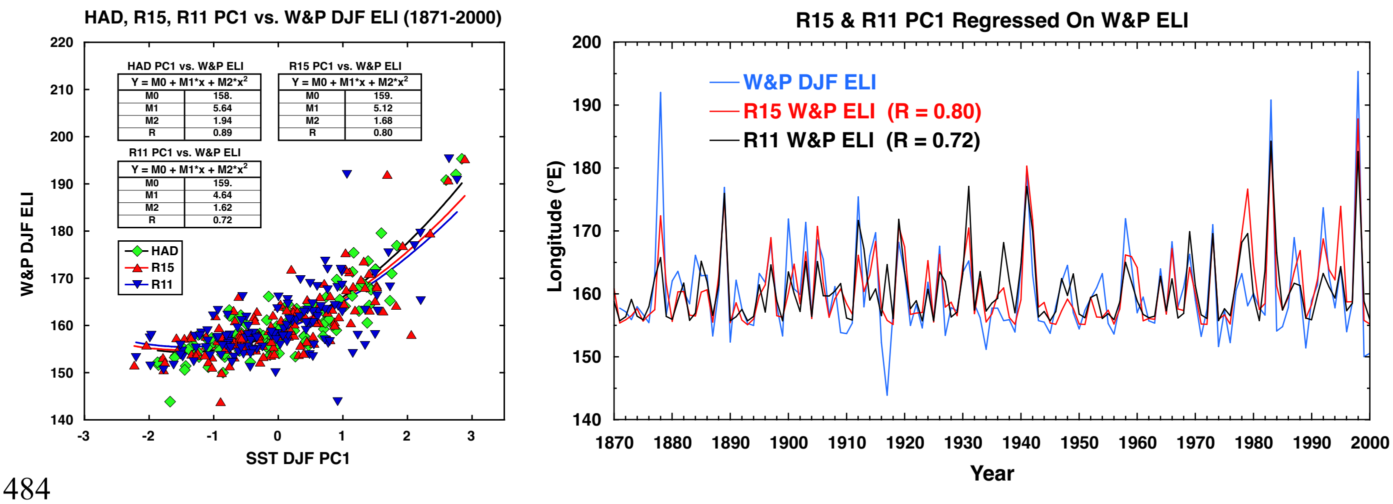

Figure S6. Williams and Patricola (2018; W&P) ELI has a strong quadratic relationship with HAD, R15, and R11 PC1s (left-hand plot). Given these strong relationships, we regressed our R15 and R11 PC1s on W&P ELI to produce reconstructions of ELI back to 1500 and 1100 shown in Figure 5 of the main paper. The estimates over the 1871-2000 calibration period are shown in the right-hand plot.

References

Cook, E. R., Meko, D. M., Stahle, D. W., & Cleaveland, M. K. (1999). Drought reconstructions for the continental United States. *Journal of Climate*, 12, 1145-1162. https://doi.org/10.1175/1520-0442(1999)012<1145:DRFTCU>2.0.CO;2

Dawdy, D. R. & Matalas, N. C. (1964). *Handbook of Applied Hydrology*. V. T. Chow (Ed.), McGraw-Hill, New York, p. 87.

Furtado, J., Di Lorenzo, E., Cobb, K. & Bracco, A. (2009). Paleoclimate reconstructions of tropical sea surface temperatures from precipitation proxies: methods, uncertainties, and nonstationarity. *Journal of Climate*, 22, 1104-1123. https://journals.ametsoc.org/view/journals/clim/22/5/2008jcli2415.1.xml.

Lenssen, N., Goddard, L. & Mason, S. (2020). Seasonal forecast skill of ENSO teleconnection maps. *Weather and Forecasting*, 35(6), 2387–2406. https://doi.org/10.1175/WAF-D-19-0235.1.

Luo, X., Dee, S., Stevenson, S., Okumura, Y., Steiger, N., & Parsons, L. (2022). Last Millennium ENSO diversity and North American teleconnections: New insights from paleoclimate Data Assimilation. Paleoceanography and Paleoclimatology, 37, e2021PA004283. https://doi.org/10.1029/2021PA004283.

Meko, D. M. (1981). *Applications of Box-Jenkins Methods of Time Series Analysis to the Reconstruction of Drought from Tree Rings*. Unpublished Ph.D. dissertation, The University of Arizona, 149 pp.

North, G., Bell, T. Cahalan, R. & Moeng, F. (1982). Sampling errors in the estimation of empirical orthogonal functions. *Monthly Weather Review*, 110(7), 699-706. https://doi.org/10.1175/1520-0493(1982)110%3C0699:SEITEO%3E2.0.CO;2.

Williams, I. & Patricola, C. (2018). Diversity of ENSO events unified by convective threshold sea surface temperature: a nonlinear ENSO index. *Geophysical Research Letters*, 45(17), 9236-9244. https://doi.org/10.1029/2018GL079203.

van Oldenborgh, G. J., Hendon, H., Stockdale, T., L'Heureux, M., Coughlan de Perez, E., Singh, R. & Aalst, M. (2021). Defining El Niño indices in a warming climate. *Environmental Research Letters*, 16(4), 044003. https://iopscience.iop.org/article/10.1088/1748-9326/abe9ed.